# AIAA 89-1833
# An Experimental Investigation of the Parallel Vortex-Airfoil Interaction at Transonic Speeds

I. Kalkhoran, D. Wilson and D. Seath
University of Texas
Arlington, TX

**AIAA 20th Fluid Dynamics, Plasma Dynamics and Lasers Conference**
Buffalo, New York / June 12–14, 1989

# AN EXPERIMENTAL INVESTIGATION OF THE PARALLEL VORTEX-AIRFOIL INTERACTION AT TRANSONIC SPEEDS

Iraj M. Kalkhoran,+ Donald R. Wilson,++ and Donald D. Seath++
The University of Texas at Arlington
Arlington, Texas 76019

## Abstract

Unsteady vortex-airfoil interaction experiments at transonic Mach numbers ranging from 0.7-0.85, and airfoil chord Reynolds numbers of 3.5-5.5 million were conducted in the UTA high Reynolds number, transonic, Ludwieg-tube wind tunnel facility. The vortex-airfoil interaction experiments were designed to simulate a two-dimensional blade-vortex interaction (BVI) problem frequently encountered in rotorcraft applications. The interaction experiments involved positioning a two-dimensional vortex generator upstream of a NACA 0012 airfoil section and impulsively pitching the vortex generator airfoil to shed a starting vortex that interacted with the downstream airfoil. Experiments were conducted at several vortex core positions above and below the downstream airfoil. The experimental results indicate a substantial change in the pressure distribution over the leading 30 percent of the interacting airfoil. Experimental data for supercritical Mach numbers indicated a very strong interaction of the vortex and the shock wave; and at close encounters these interactions resulted in unsteady local flow separation of the leading 40 percent of the airfoil chord. Experiments with stronger vortices at supercritical Mach numbers resulted in a forward propagation of the shock wave. The experimental results also indicated that the pressure distribution of the downstream airfoil was not sensitive to Reynolds number variations.

## Nomenclature

a Speed of sound
c Chord length
$C_\ell$ Lift coefficient
$C_p$ Pressure coefficient $\frac{p - p_\infty}{\frac{1}{2}\rho_\infty u_\infty^2}$
h Vortex generator height with respect to airfoil leading edge
k Reduced frequency, $\frac{\dot{\alpha} c}{u_\infty}$
M Mach number
p Pressure
T Time
u Velocity
x Chord position
$\alpha$ Angle of attack
$\dot{\alpha}$ Angular velocity
$\Gamma$ Circulation
$\bar{\Gamma}$ Non-dimensional vortex strength, $\Gamma / u_\infty c$
$\Lambda$ Vortex intersection angle (Fig. 1)
$\rho$ Density

Subscripts
t Total
v Vortex
$\infty$ Free-stream

## Introduction

The interaction of the tip vortex shed from one blade with the other blades of a helicopter rotor is known to have a marked effect on both the aerodynamic and acoustic characteristics of the helicopter. The Blade-Vortex Interaction (BVI) has been identified as the source of unsteady aerodynamic loading of the blades, as well as the acoustic phenomenon known as "blade slap" (Ref. 1). The blade-vortex interaction is most likely to occur during a powered descent, and in general, consists of an interaction of curved-line vortices with a lifting surface at an arbitrary intersection angle. The limiting cases are represented by the parallel (axis of vortex parallel with the leading edge of the blade) and perpendicular (axis of vortex perpendicular to the leading edge of the blade) interactions (Fig. 1). The parallel BVI is essentially a two-dimensional, unsteady flow problem, whereas the perpendicular BVI is usually considered as a steady but highly three-dimensional flow.

Previous investigations of the BVI problem have generally focused on either the perpendicular or parallel interaction; and although the most pronounced effects occur at transonic speeds, most of the studies have concentrated on the aeroacoustics of BVI at relatively low speeds (Refs. 2-7). The perpendicular BVI problem was studied experimentally by Ham (Ref. 2), Schlinker and Amiet (Ref. 3), Ahmadi (Ref. 4), and Seath and Wilson (Ref. 5). The studies reported by Ham (Ref. 2) and Seath and Wilson (Ref. 5) focused on the aerodynamic aspects of the perpendicular BVI and included detailed surface pressure measurements. Both reported a significant alteration of the pressure distribution as a result of the proximity of the vortex. Furthermore, the effect was most pronounced near the leading edge of the airfoil. The investigation of the perpendicular BVI at transonic speeds was reported by Wilson, Kalkhoran and Seath in Ref. 8. In general, the phenomena observed at transonic flow conditions were found to be qualitatively similar to those observed at lower speeds, however the relative impact on the airfoil pressure distribution was increased considerably compared to the low speed results.

The low-speed aerodynamic aspects of the parallel blade-vortex interaction were reported by Seath, Kim and Wilson (Ref. 6) and Straus, Renzoni and Mayle

* Work supported by ARO Grant DAAG29-84-K-0131, Dr. Thomas L. Dolagalski, contract monitor.
+ Visiting Assistant Professor, Aerospace Engineering Department, Member, AIAA
++ Professor, Aerospace Engineering Department, Associate Fellow, AIAA

(Ref. 7). Their scheme involved placing a vortex generator upstream of a two-dimensional airfoil and "impulsively" pitching the vortex generator such that its starting vortex interacted with the downstream airfoil. Their results indicated a significant alteration of the pressure distribution during the interaction, with the most pronounced effects concentrated near the leading edge of the airfoil. Caradonna, Laub and Tung (Ref. 9) investigated the parallel BVI by mounting an instrumented rotating blade downstream of a vortex generator in a low speed wind tunnel. The blade RPM was set to simulate the parallel BVI at transonic relative Mach numbers. Two propagation mechanisms were observed in their experiments; a "type C" shock propagation at high tip speeds, and a rapid but continuous pressure pulse associated with the proximity of the vortex at lower tip speeds. Another technique for simulating the parallel BVI is reported by Meier and Timm (Ref. 10) and Mandella and Bershader (Ref. 11) in which the vortices are generated by the impulsive starting of the flow over an airfoil mounted at an angle of attack in a shock tube. In their experiments, flow visualization via high speed interferometry as well as side wall pressure measurements were used to quantify the vortex intensity and the details of the interaction. Their results indicate a substantial transient disturbance to both lift and drag of the downstream airfoil.

The present investigation was designed to measure the unsteady surface pressure distribution on an airfoil during a parallel BVI encounter. The vortex was generated by impulsively pitching a full-span NACA 0012 airfoil section to shed a starting vortex, and allowing this vortex to convect downstream and interact with a second instrumented 0012 airfoil. The experiments were conducted in the UTA High-Reynolds Number, Ludwieg-Tube Wind Tunnel (Ref. 12) at transonic Mach numbers and at Reynolds numbers representative of actual helicopter flight operations.

## Experimental Setup

A line drawing of the transonic Ludwieg-tube wind tunnel is shown in Fig. 2a, and a cross-sectional view of the nozzle, test section, diffuser, and start valve is shown in Fig. 2b. The tunnel has an 18.5 x 23.3 cm (7.34 x 9.16 in) porous wall test section, and is capable of producing low-turbulence transonic flows at Mach numbers of 0.5-1.2, and unit Reynolds numbers up to $4(10)^8$ per meter (10 million/inch).

The vortex generator consisted of a NACA 0012 airfoil section having a 5.08 cm (2 in) chord that was mounted to a pitch actuation mechanism located at the interface between the nozzle and test section. The vortex generator airfoil was mounted vertically at the tunnel centerline and spans the entire height of the test section. The vortex generator is impulsively pitched during the steady state portion of the wind tunnel run by means of a high speed Tomkins-Johnson model SH-2 pneumatic actuator. A potentiometer was attached to the actuator in order to measure the actual pitch angle time history of the vortex generator. Maximum pitch rates of about 20 rad/sec could be achieved with this system, which corresponds to a reduced frequency, $k = \dot{\alpha}c/u_\infty$, of the order of 0.005.

An instrumented NACA 0012 airfoil section with a 5.08 cm (2 in) chord length, also spanning the entire height of the test section, was mounted vertically 43.18 cm (17 in) downstream of the vortex generator airfoil. The model has approximately 3.2 percent blockage in the test section. The airfoil is equipped with 8 fast response surface mounted Kulite LQ-080-100 pressure transducers. The pressure transducers are located along the airfoil chord at every 0.1 c, with the first transducer at the 10 percent chord station and the last transducer at the 80 percent chord station. Due to the size limitations of the model, the airfoil was instrumented on one side only (Fig. 3).

The end plates of the downstream interacting airfoil were designed such that it could be positioned at various horizontal locations in the test section. Since the vortex generator was always located at the tunnel centerline, by positioning the downstream airfoil at various locations off centerline, vortex-airfoil interactions with different incident separation distances could be accomplished.

Facility operation, control, and data acquisition are accomplished by means of a DSP Technology high-speed data acquisition and control system (Fig. 4). The DSP Technology system provides 48 channels for data acquisition (pressure transducer, strain-gage, or thermocouple input) and 16 output channels for facility control. The system employs a simultaneous sample-and-hold concept, and provides simultaneous sampling of all 48 channels at a maximum sampling frequency of 100 KHz/channel. Each channel has its own dedicated variable gain amplifier, 12-bit A/D converter, and on-line memory bank for storage of the digitized signals during a test run. The data are then transferred through a National Instruments GPIB bus to a master computer located in the control room for subsequent data reduction and analysis.

## Calibration Experiments

The wind tunnel calibration procedure consisted of simultaneous measurements of the charge tube stagnation pressure with total pressure probes located at the downstream end of the charge tube, the test section static pressure distribution with a standard centerline pipe, and the test section plenum cavity pressure with a plenum cavity rake. Details of the procedure are given in Refs. 8 and 13. The axial variation of test section Mach number is about 0.5 percent for the range of Mach numbers tested.

The airfoil calibration experiments were conducted for Mach numbers ranging from 0.7 to 0.85, and Reynolds numbers of 3.5 and 5.5 million based on the airfoil chord. The specific objectives of the airfoil calibration experiments were to verify the accuracy and repeatability of the airfoil pressure distribution, and also to obtain a set of baseline data to be compared to

the pressure distribution data during the unsteady vortex-airfoil interaction experiments.

The major difficulty encountered during the airfoil calibration studies was the deviation of the baseline pressure distribution from published experimental data for the NACA 0012 section. The reason for this discrepancy is believed to be a result of surface irregularities caused by the surface mounted pressure transducers. The discrepancy tends to be more pronounced near the leading edge of the airfoil due to the higher curvature in that region. Considering the sensitivity of the airfoil pressure distribution to small surface irregularities at transonic Mach numbers, only the vortex effects on the pressure distribution of the existing model will be presented, and the discussion will focus on the deviation of measured surface pressures from the baseline values.

## Experimental Results

The vortex-airfoil interaction tests were conducted at 5 incident vortex generator-airfoil vertical separation distances, as shown in Fig. 5. The vortex generator was pitched counterclockwise about the quarter-chord point, thus leading to trajectories of the shed starting vortex that include both passage over the upper surface (cases A and B) and below the lower surface (Cases C, D and E). Only the lower surface of the airfoil is instrumented with pressure transducers. The maximum pitch angle for these cases was $\alpha = +5°$, which corresponds to an estimated non-dimensional vortex strength of,

$$\bar{\Gamma}_v = \Gamma_v / \left( u_\infty c \right) = \frac{1}{2} C_\ell = 0.25 \qquad (1)$$

Time history plots of the amplified pressure transducer output for $x/c = 0.1$, 0.2, and 0.3 along with a superposition of the output signal from the vortex generator pitch angle sensor are shown in Fig. 6 for cases A-E at a nominal Mach number of 0.72. In some instances (cf Fig. 6.c) a small increase in pressure near the leading edge is observed on the order of 0.7 ms after initiation of the pitch maneuver, which corresponds roughly to the convection time for acoustic waves traveling with a propagation speed of $u_\infty + a$ to reach the downstream airfoil. A similar drop in pressure starts about 0.7 ms after termination of the pitch maneuver and reaches a minimum value about 1.7 ms after termination of the pitch maneuver. This later time interval roughly corresponds to the convection time for disturbances propagating with the local flow speed $u_\infty$ to reach the downstream airfoil. This minimum pressure is then followed by a rapid compression over the leading portion of the airfoil. It is postulated that the starting vortex is shed from the vortex generator at the termination of the pitch maneuver, and convects downstream at the local flow velocity, reaching the leading edge of the downstream airfoil 1.7 ms later. This vortex shedding model appears to be substantiated by flow visualization experiments conducted at low speeds (Ref. 6) and by CFD simulations of the transient flow field about a pitching airfoil conducted by Jones (Ref. 14) for a NACA 0012 airfoil at the same Mach number, Reynolds number and reduced frequency.

Cases A and B (Fig. 6.a, 6.b) represent cases for which the vortex passes over the upper surface of the downstream airfoil. The time history plots indicate a slight drop in pressure as the vortex approaches the airfoil, followed by a rapid increase in pressure to a value higher than the undisturbed pressure level as the vortex passes over the airfoil. The pressure distribution then oscillates as a result of induced flow oscillations caused by vibration of the vortex generator upon impact with the mechanical stop on the pitch actuation mechanism that is used to set the maximum pitch angle. The effect of the vortex passage is seen to be most pronounced at $x/c = 0.1$ and 0.2, with relatively little effect observed downstream of the 20 percent chord station.

The geometry of the parallel BVI encounter represented by cases C, D and E (Fig. 6.c, 6.d and 6.e) corresponds to the classic configuration of a clockwise-rotating vortex passing under the lower surface of a rotor blade that has been extensively reported in the BVI literature. Case C represents the closest encounter, and the pressure distribution is seen to consist of a rather strong drop in pressure near the leading edge of the airfoil as the vortex approaches, followed by a rapid increase in pressure as the vortex passes under the airfoil. Again, the effect is seen to be most pronounced near the leading edge of the airfoil, which is in qualitative agreement with the low-speed test results of Seath, et al (Ref. 6) and the transonic-flow experiments of Caradonna, et al (Ref. 9). This is in contrast to reported results based on CFD simulations of the parallel BVI at transonic speeds (Refs. 15,16). The CFD simulations suggest similar time-histories near the leading edge of the airfoil but predict a more uniform chord-wise extent of the vortex-induced pressure change over the entire airfoil. Cases D and E are geometrically similar to Case C, but for increased vertical separation distance between the vortex core and the airfoil. Except for the rather large increase in pressure at $x/c = 0.1$ prior to termination of the vortex generator pitch maneuver that is observed in Case D, the results are qualitatively similar. The reason for this increase in pressure is not well-understood at the present time.

The time history pressure traces discussed above are presented in the form of the airfoil pressure coefficient distribution in Figs. 7.a and 7.b, for cases C and D respectively. The above figures do indeed verify that most of the airfoil interaction effects are concentrated near the leading 30 percent of the airfoil chord. Figure 7.a shows the instantaneous pressure distribution for a period of 3.75 ms. The initial $C_p$ distribution at T = 28 ms corresponds to the undisturbed pressure distribution approximately 0.4 ms before the completion of the pitch motion. A gradual decrease in the pressure coefficients at $x/c = 0.1$, 0.2 and 0.3 is quite evident, while downstream of $x/c = 0.4$, it seems that the pressure distributions are not affected by the passage of the vortex. At T = 30 (about 1.6 ms after the completion of the pitch motion) the airfoil pressure

distribution indicates a rather substantial decrease in the $C_p$ near the x/c = 0.1 station, in comparison to its "undisturbed" value at T = 28 ms. Beyond T = 30.75 ms, the general trend is in the direction of recovering from the unsteady disturbances. However, as indicated earlier, due to the vibration of the vortex generator the complete recovery is not reached for quite sometime. A more pronounced effect on the airfoil pressure distribution is shown in Fig. 7.b, for the case in which the downstream airfoil is in position D. Again a progressive decrease in the magnitude of the $C_p$ values near the leading edge of the airfoil is evident. This trend starts at T = 28.5 ms, approximately 0.7 ms before the completion of the pitch motion, and continues until T = 30.8 (about 1.7 ms after the completion of the pitch maneuver), at which time the pressure distribution near the leading edge of the airfoil undergoes compression in the general direction of recovering from the unsteady disturbances.

Experiments with higher free stream Mach numbers resulted in an interaction with higher intensity than the cases discussed above. The time history of the local Mach numbers at x/c = 0.1, 0.2, 0.3 and 0.4 for the downstream airfoil positions corresponding to cases B, C and D are presented in Figs. 8.a through 8.c respectively. The above Mach number traces for cases C and D indicate a strong decrease in the local Mach number at the 30 percent chord location just upstream of the steady-flow shock wave position, which is an indication of the interaction of the unsteady vortex with the shock wave. Similar to the lower free stream Mach number runs, the supercritical cases resulted in the most pronounced interactions when the vortex passed under the airfoil.

The pressure distribution data for the case in which the downstream airfoil was at position C are illustrated in Fig. 9a. It may be seen that from T = 29.6 ms (0.9 ms after the completion of the pitch motion) until T = 30.4, the strong shock wave at x/c = 0.4 appears to move upstream to a new location at x/c = 0.3 with a substantial loss in the strength of the shock wave. It may also be seen that this is to a large degree a local effect and only the $C_p$ values just upstream and downstream of the shock wave are affected by this shock motion. It is also interesting to note that after about 1.2 ms, the airfoil pressure distribution is essentially the same as its undisturbed value. A similar behavior may be observed in Fig. 9.b for case D.

The forward propagation of the shock wave during the interaction was found to be more pronounced if the vortex generator was pitched from a preset negative angle to a positive angle of attack. This maneuver should shed a vortex with a nondimensional strength $\bar{\Gamma}_v$ of 0.5, for a pitch excursion from -5 to +5 degrees. An example of such a case is presented in Fig. 10. Figure 10.a illustrates the time history plots of the local Mach numbers for x/c = 0.1 through x/c = 0.4. Although the picture is complicated by the presence of a weak shock wave at x/c = 0.2, it is apparent that a sharp decrease in the local Mach number at x/c = 0.3 occurs approximately 0.7 ms before the disturbances are felt at x/c = 0.1. The pressure coefficient distribution of Fig. 10.a is illustrated in Fig. 10.b for a period of 3 ms. At T = 30 ms the undisturbed pressure distribution indicates a very strong shock wave at x/c = 0.4. At T = 31.5 ms, the shock wave has moved upstream to x/c = 0.3 with a substantial loss in its strength, while the aft portion of the airfoil does not seem to be affected by the interaction. At T = 32.2 ms the distribution is very similar to the undisturbed values before a second disturbance results in another upstream shock movement, leading to compression of the leading portion of the airfoil. This leads to a pattern of unsteady flow separation and reattachment near the airfoil leading edge (T = 33 ms), and a complete recovery of the pressure distribution to its initial undisturbed condition is not seen.

The variation of Reynolds number, as shown in Fig. 11, does not appear to have a significant effect on the downstream airfoil. Figure 11 illustrates the Mach number traces for M = 0.77 at x/c = 0.1, 0.2, 0.3 and 0.4 and chord Reynolds numbers of 3.8 and 5.4 million. Except for minor differences in time correlation of the large-amplitude pressure variations at x/c = 0.3, the traces are essentially identical.

## Conclusions

The results of the present investigation indicated that the unsteady interaction of a vortex with a two dimensional airfoil can have a significant effect on the pressure distribution of the interacting airfoil. The experimental results are qualitatively similar to the pressure distributions obtained from CFD simulations of the interactions for sub-critical and critical Mach numbers with one notable exception; the experimental results indicate that the interaction is more pronounced over the leading 40 percent of the airfoil chord, whereas the CFD simulations suggest a more uniform cord-wise extent of the interaction. Experimental data for free-stream Mach numbers representing supercritical flow over the airfoil indicate that a strong interaction between the vortex and the airfoil shock wave can lead to shock wave oscillation and local flow separation. For this condition, an increase in the strength of the vortex was seen to produce a forward propagation of the shock wave (Class-C shock motion). In general, the effect of Reynolds number variation over the range tested appears to be of second order.

## References


1. George, A. R., "Helicopter Noise: State-of-the-Art," AIAA J. Aircraft, Vol. 15, No. 11, pp. 707-715, Nov. 1978.
2. Ham, N. D., "Some Conclusions from an Investigation of Blade-Vortex Interaction," J. of American Helicopter Society, Vol. 20, No. 4, pp. 26-31, Oct. 1976.
3. Schlinker, R. H. and Amiet, R. K., "Rotor-Vortex Interaction Noise," AIAA Paper 83-0720, AIAA 8th Aeroacoustics Conference, Atlanta, GA, April 11-13, 1983.
4. Ahmadi, A. R., "An Experimental Investigation of Blade-Vortex Interaction at Normal Incidence,"

Workshop on Blade-Vortex Interactions, NASA-Ames Research Center, CA, Oct. 1984.
5. Seath, D. D. and Wilson, D. R., "Vortex-Airfoil Interaction Tests," AIAA Paper 86-0354, AIAA 24th Aerospace Sciences Meeting, Reno, NV, Jan. 1986.
6. Seath, D. D., Kim, J. M. and Wilson, D.R., "An Investigation of the Parallel Blade-Vortex Interaction in a Low-Speed Wind Tunnel," AIAA Jour. Aircraft, Vol. 26, No. 4, April 1989, pp. 328-333.
7. Straus, J., Renzoni, P. and Mayle, R.E., "Airfoil Pressure Measurements During a Blade-Vortex Interaction and a Comparison with Theory," AIAA Paper 88-0669, AIAA 26th Aerospace Sciences Meeting, Reno, NV, Jan. 1988.
8. Wilson, D. R., Kalkhoran, I. M. and Seath, D. D., "An Experimental Investigation of the Perpendicular Vortex-Airfoil Interaction at Transonic Speeds," AIAA Paper 87-0208, AIAA 25th Aerospace Sciences Meeting, Reno, NV, Jan. 1987.
9. Caradonna,F. X., Laub, G. H. and Tung, C., "An Experimental Investigation of the Parallel Blade-Vortex Interaction," Paper No. 4, 10th European Rotorcraft Forum, The Hague, Netherlands,Aug. 1984.
10. Meier, G. E. A. and Timm, R., "Unsteady Vortex Airfoil Interaction," AGARD CP-386, May 1985.
11. Mandella, M and Bershader, D., "Quantitative Study of the Compressible Vortex: Generation, Structure and Interaction with Airfoils," AIAA Paper 87-0328, AIAA 25th Aerospace Sciences Meeting, Reno, NV, Jan. 1987.
12. Wilson, D. R. and Chou, S. Y., "Development of the UTA High Reynolds Number Transonic Wind Tunnel," AIAA Paper 85-0315, AIAA 23rd Aerospace Sciences Meeting, Reno, NV, Jan. 1985.
13. Kalkhoran, I. M., "An Experimental Investigation of the Perpendicular Vortex-Airfoil Interaction at Transonic Speeds," Ph.D. Dissertation, The University of Texas at Arlington, Dec. 1987.
14. Jones, H. E., NASA-Langley Research Center, Private Communication, Aug. 1988.
15. Srinivasan, G.R., McCroskey, W. J. and Kutler, P., "Numerical Simulation of the Interaction of a Vortex with Stationary Airfoil in Transonic Flow," AIAA 84-0254, AIAA 22th Aerospace Sciences Meeting, Reno, NV, Jan. 9-12, 1984.
16. Jones, H. E., "The Aerodynamic Interaction Between an Airfoil and a Vortex in Transonic Flow," Paper presented at ARO Workshop on Blade-Vortex Interaction, NASA Ames Research Center, CA, Oct. 1984.

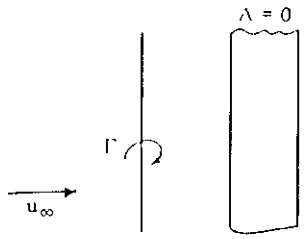


(a) Vortex parallel to leading edge

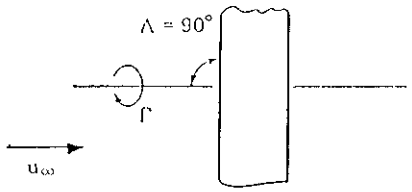


(b) Vortex perpendicular to leading edge

Fig. 1. Parallel and perpendicular blade-vortex interactions

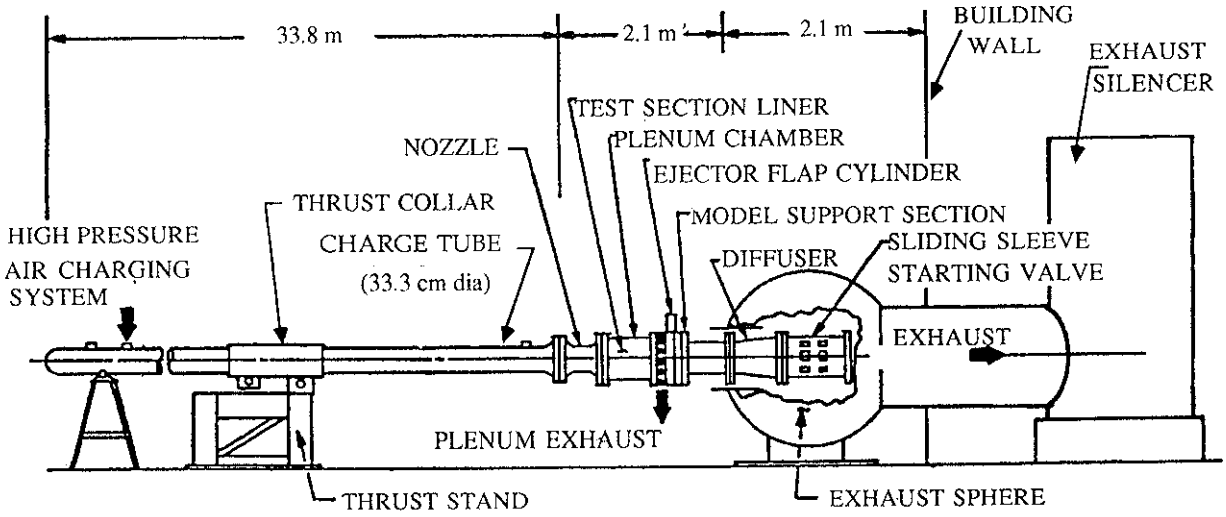


(a) Elevation view

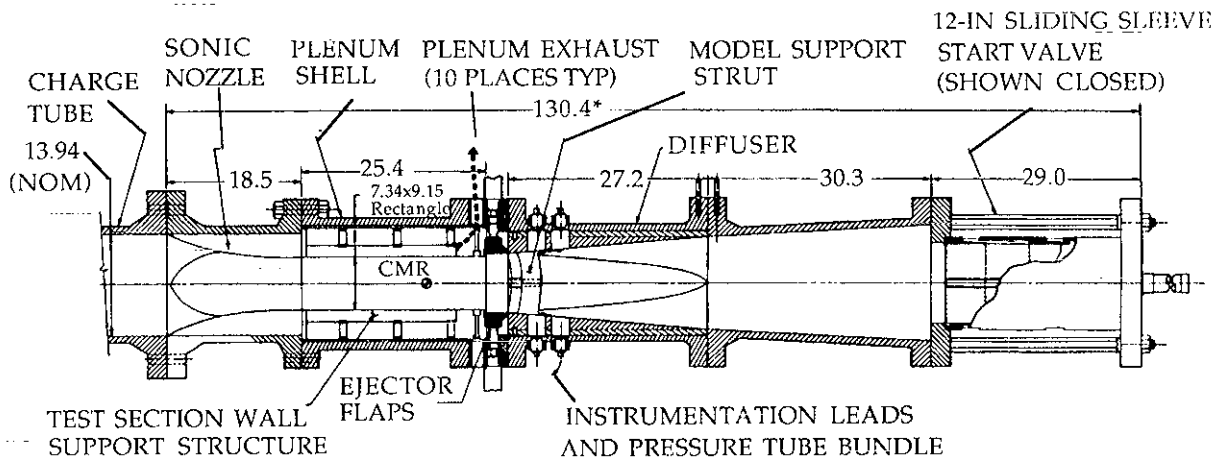


(b) Cross sectional view of nozzle, test section, diffuser and main valve system

Fig. 2. Transonic Ludwieg-tube wind tunnel

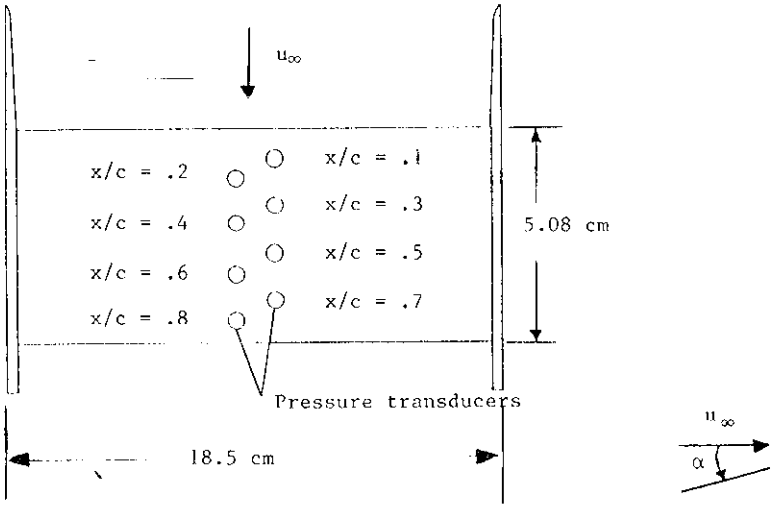


Fig. 3. Downstream airfoil geometry and transducer locations

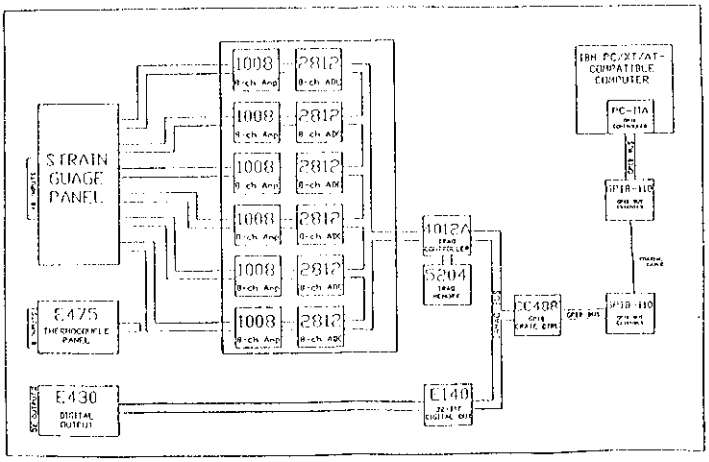


Fig. 4. Data acquisition and control computer system

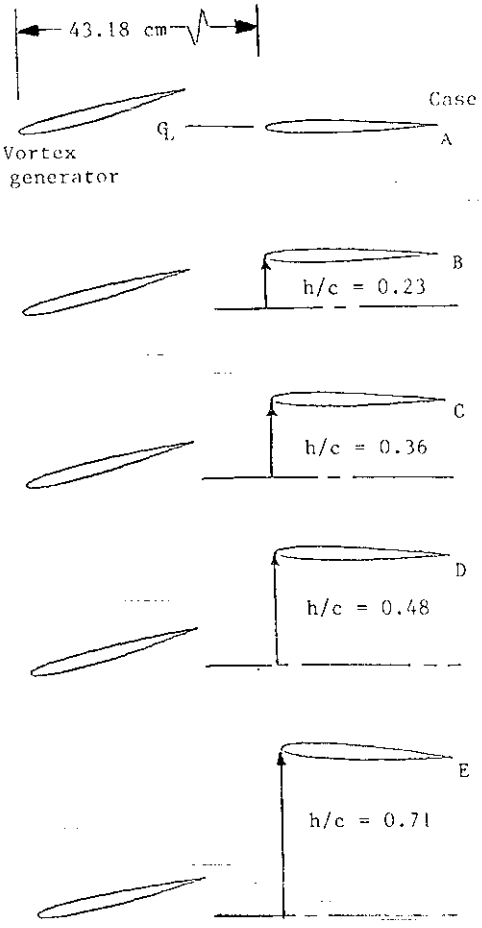


Fig. 5. Vortex-airfoil interaction geometry

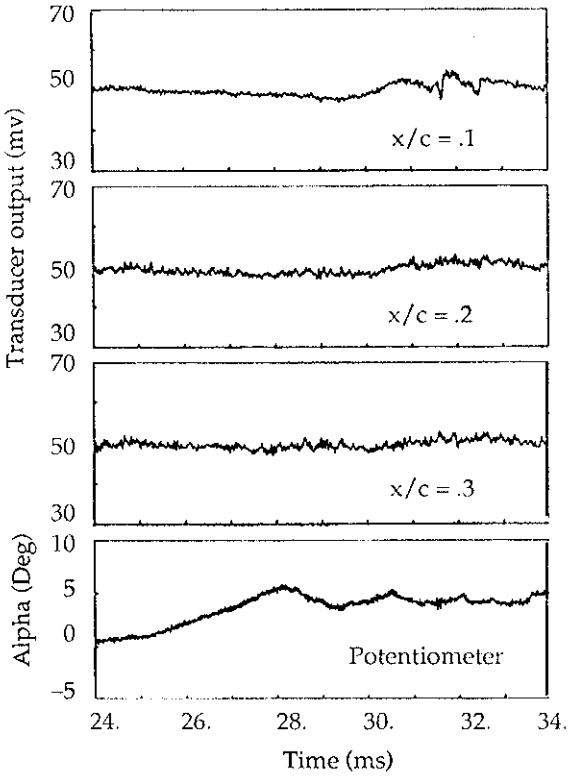


(a) Case A: M = 0.71, Re =3.8 x $10^6$, h/c = 0

Fig. 6. Time history of pressure signals during the vortex-airfoil interaction

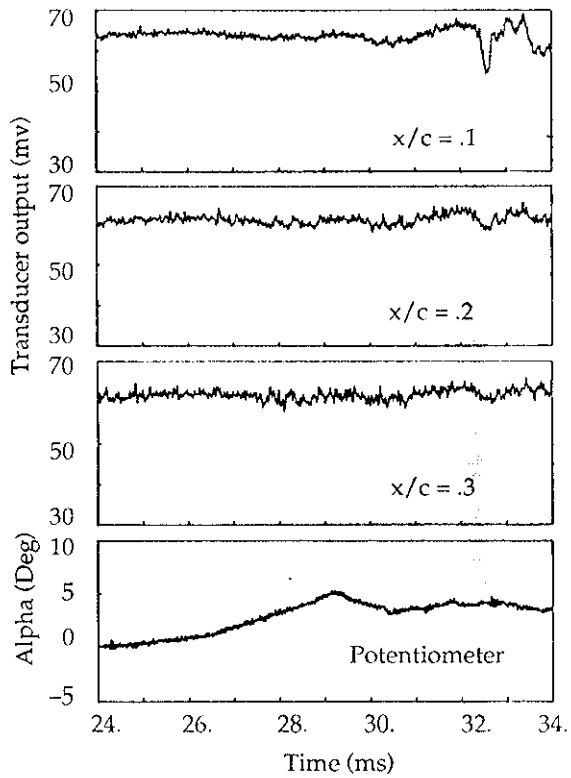


(b) Case B: M = 0.72, Re = 5.4 x $10^6$, h/c = 0.23

Fig. 6 (Continued)

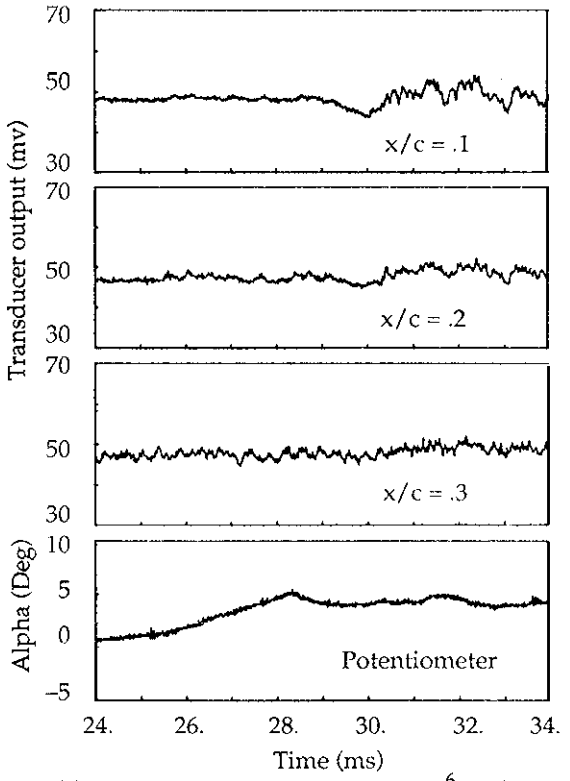


(c) Case C: M = 0.72, Re = 3.4 x $10^6$, h/c = 0.36

Fig. 6 (Continued)

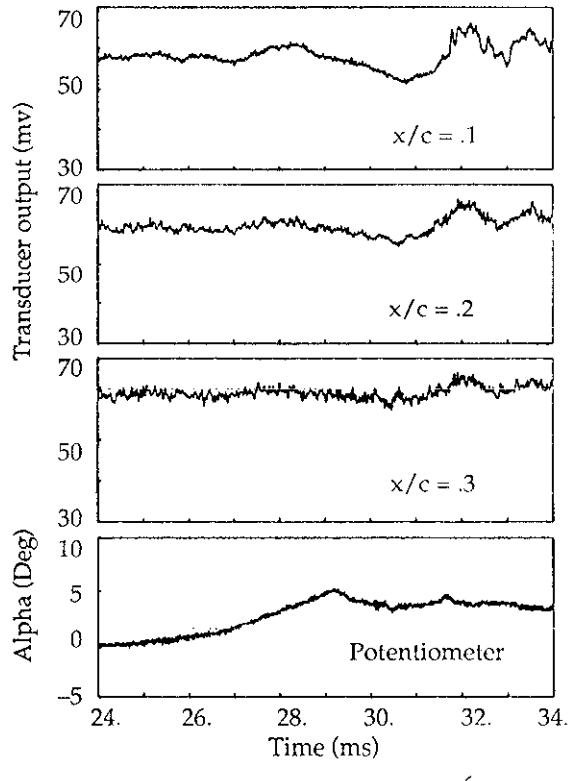


(d) Case D: M = 0.72, Re = 3.8 x $10^6$, h/c = 0.48

Fig. 6 (Continued)

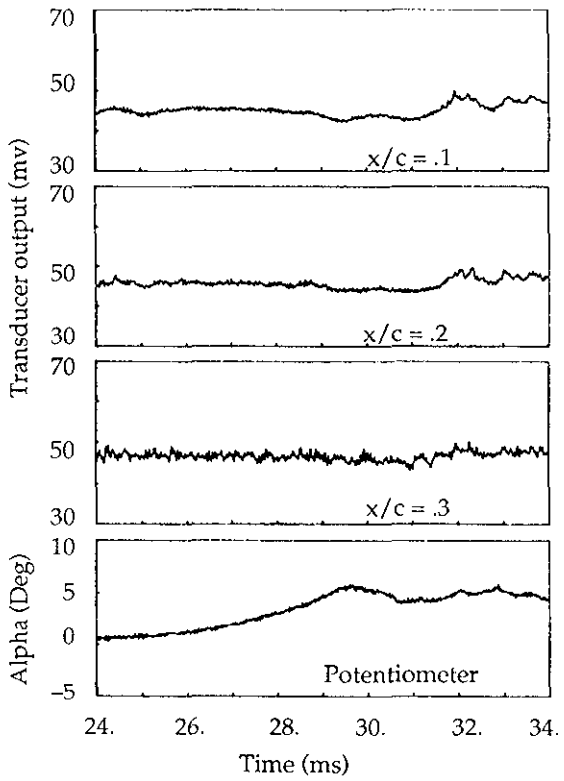


(c) Case E: M = 0.72, Re = $3.4 \times 10^6$, h/c = 0.71

Fig. 6 (Concluded)

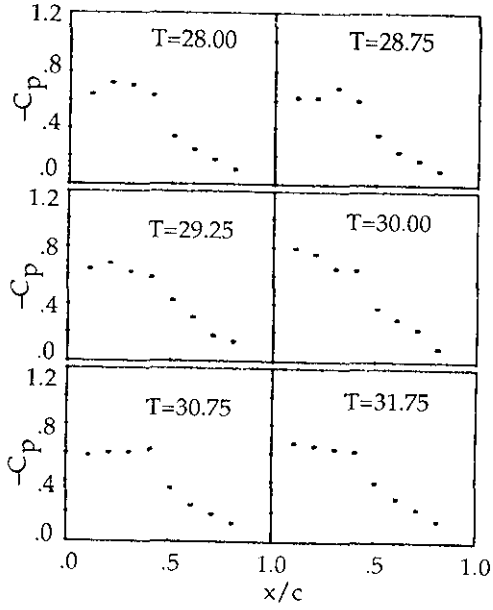


(a) Case C: M = 0.72, Re = $3.4 \times 10^6$, h/c = 0.36

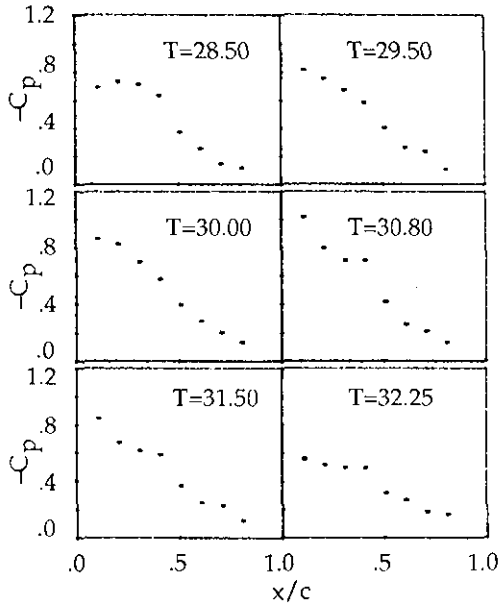


(b) Case D: M = 0.72, Re = $3.8 \times 10^6$, h/c = 0.48

Fig. 7. Pressure coefficient distribution during the vortex-airfoil interaction

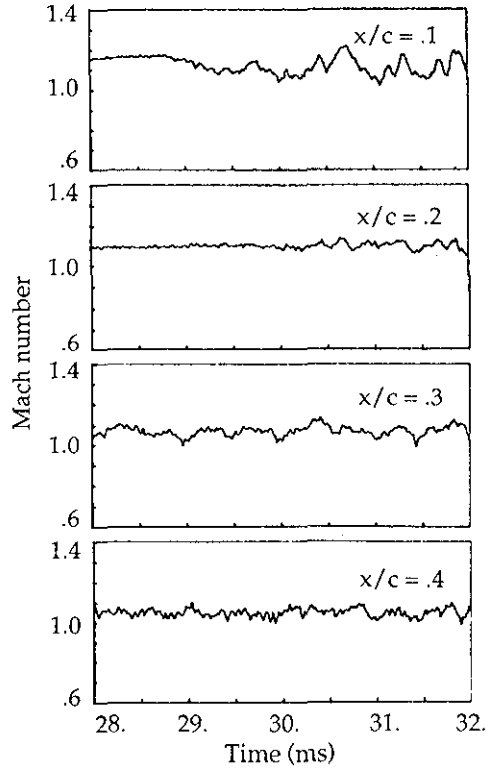


(a) Case B: M = 0.77, Re = $5.4 \times 10^6$, h/c = 0.23

Fig. 8. Time history of local Mach number distribution

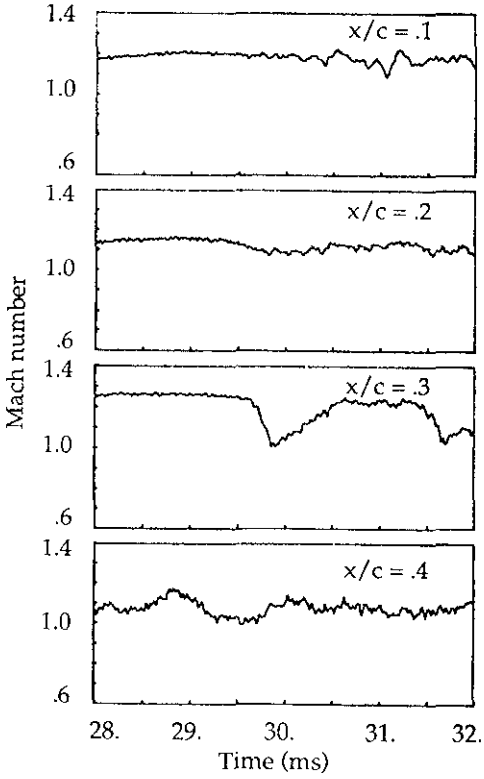


(b) Case C: M = 0.77, Re =3.8 x $10^6$, h/c = 0.36

Fig. 8. (Continued)

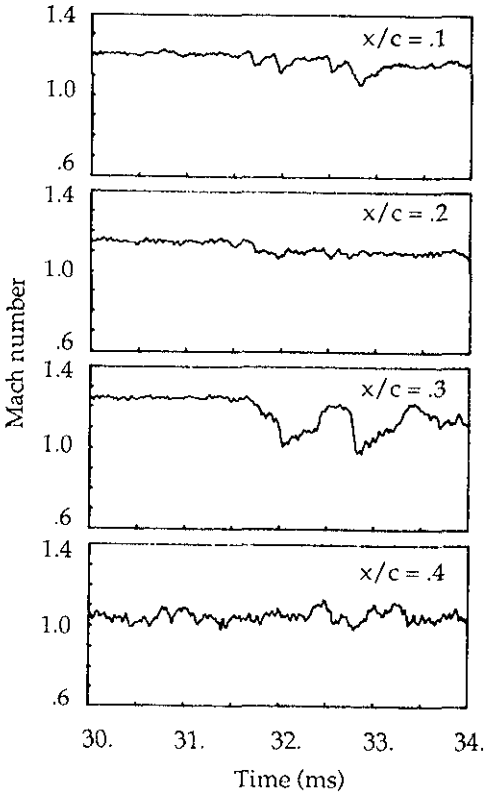


(c) Case D: M = 0.78, Re = 3.8 x $10^6$, h/c = 0.48

Fig. 8. (Concluded)

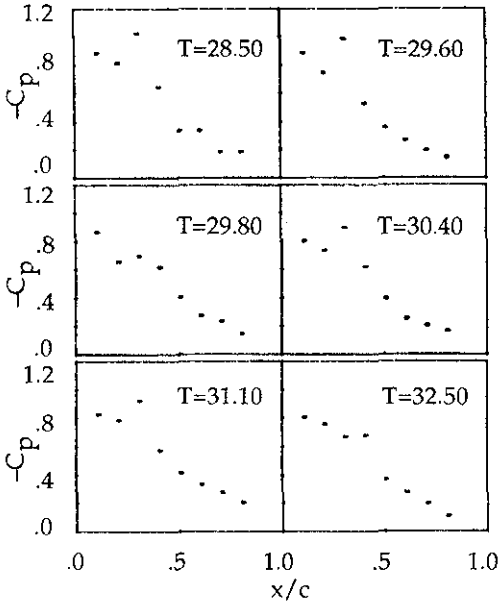


(a) Case C: M = 0.77, Re = 3.8 x $10^6$, h/c = 0.36

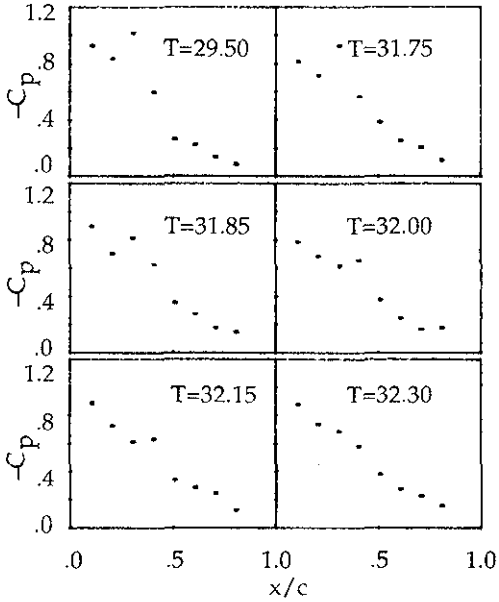


(b) Case D: M = 0.78, Re = 3.8 x $10^6$, h/c = 0.48

Fig. 9. Pressure coefficient distribution during the vortex-airfoil interaction, supercritical flow

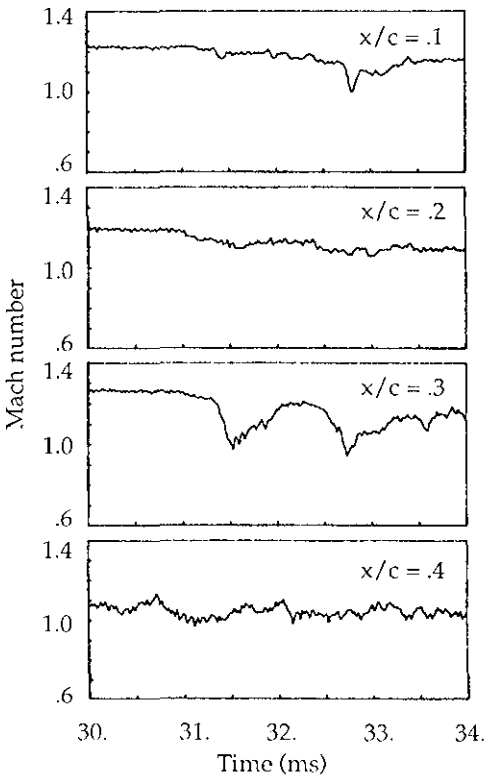


(a) Mach number

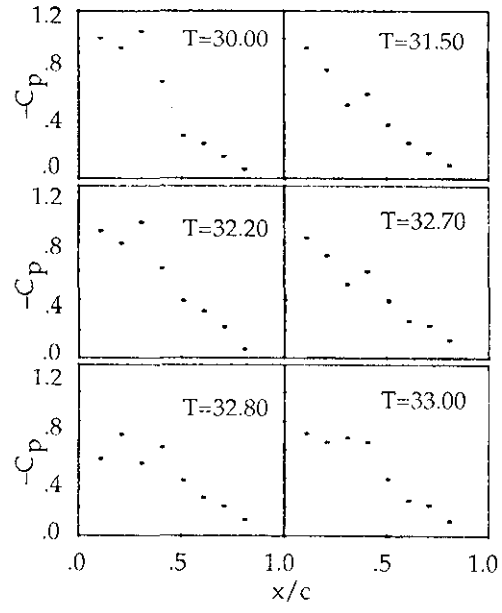


(b) Pressure coefficient

Fig. 10. Time history of local Mach number and pressure coefficient distribution; M = 0.77, Re = $3.8 \times 10^6$, $\Delta\alpha = 10°$, h/c = 0.36

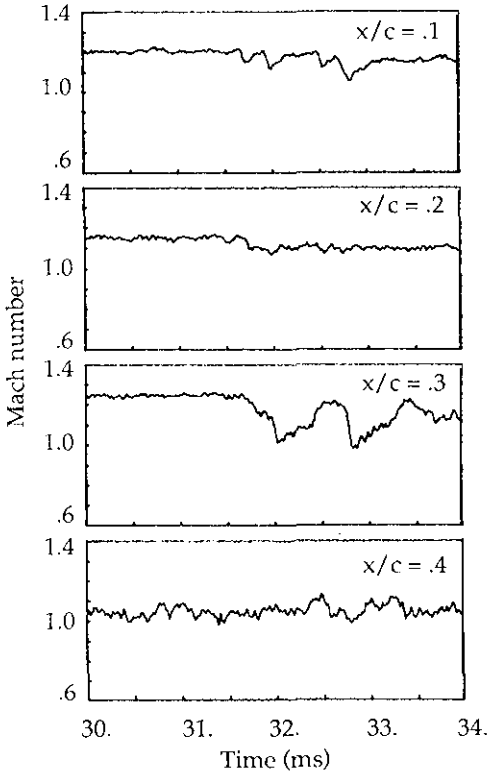


(a) Re = $3.8 \times 10^6$

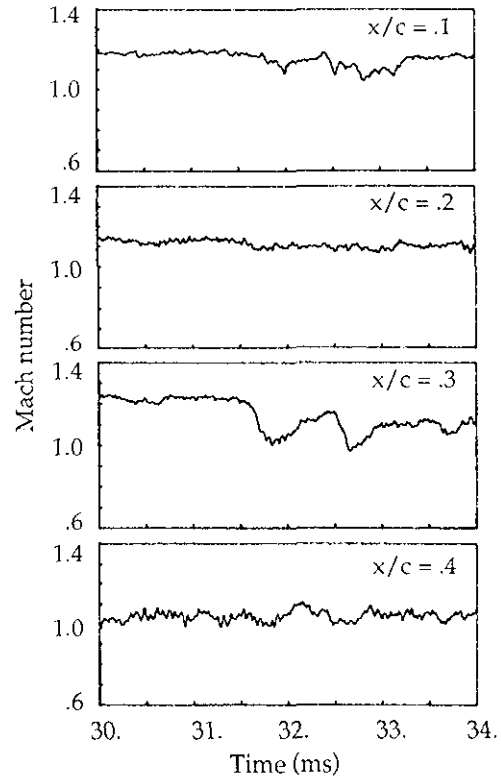


(b) Re = $5.4 \times 10^6$

Fig. 11. Illustration of Reynolds number effect; M = 0.77, h/c = 0.48